

University of Texas Rio Grande Valley

ScholarWorks @ UTRGV

Mechanical Engineering Faculty Publications
and Presentations

College of Engineering and Computer Science

2-3-2021

Defect detection in freight railcar tapered-roller bearings using vibration techniques

Constantine Tarawneh

The University of Texas Rio Grande Valley

Joseph Montalvo

The University of Texas Rio Grande Valley

Brent Wilson

Follow this and additional works at: https://scholarworks.utrgv.edu/me_fac



Part of the [Mechanical Engineering Commons](#), and the [Transportation Engineering Commons](#)

Recommended Citation

Tarawneh, C., Montalvo, J. & Wilson, B. Defect detection in freight railcar tapered-roller bearings using vibration techniques. *Rail. Eng. Science* (2021). <https://doi.org/10.1007/s40534-020-00230-x>

This Article is brought to you for free and open access by the College of Engineering and Computer Science at ScholarWorks @ UTRGV. It has been accepted for inclusion in Mechanical Engineering Faculty Publications and Presentations by an authorized administrator of ScholarWorks @ UTRGV. For more information, please contact justin.white@utrgv.edu, william.flores01@utrgv.edu.



Defect detection in freight railcar tapered-roller bearings using vibration techniques

Constantine Tarawneh¹ · Joseph Montalvo¹ · Brent Wilson²

Received: 31 August 2020 / Revised: 13 December 2020 / Accepted: 22 December 2020
© The Author(s) 2021

Abstract Currently, there are two types of defect detection systems used to monitor the health of freight railcar bearings in service: wayside hot-box detection systems and trackside acoustic detection systems. These systems have proven to be inefficient in accurately determining bearing health, especially in the early stages of defect development. To that end, a prototype onboard bearing condition monitoring system has been developed and validated through extensive laboratory testing and a designated field test in 2015 at the Transportation Technology Center, Inc. in Pueblo, CO. The devised system can accurately and reliably characterize the health of bearings based on developed vibration thresholds and can identify defective tapered-roller bearing components with defect areas smaller than 12.9 cm² while in service.

Keywords Railcar health monitoring · Onboard condition monitoring systems · Bearing defect detection · Bearing vibration signatures · Bearing spectral analysis

1 Introduction

The cargo load of each freight railcar is supported by the railcar's suspension components: springs, dampers, axles, wheels, tapered-roller bearings, and side frames. Of these components, the bearings are the most susceptible to failure due to the heavy cargo loads they support at high speeds.

The tapered-roller bearing typically used in freight railcar service has three distinct fundamental components: rollers, inner rings (cones), and outer ring (cup). These components, shown in Fig. 1, allow for near-frictionless operation under heavy loads and high speeds. However, when one of these components develops a defect, the operational effectiveness is compromised, which may lead to increased frictional heating depending on the size and location of the initiated defect.

The defects can be categorized into one of three general categories: a geometric defect, a localized defect, or a distributed defect. A geometric defect is when one or more of the fundamental components of the bearing are out of tolerance because of inconsistencies in the manufacturing processes. A bearing can also develop a geometric defect through improper reconditioning or prolonged usage. Two examples of localized defects that include pits, cracks, or spalls on a single component of the bearing are illustrated in Fig. 2 (left). A distributed defect is when multiple bearing components have localized defects or a single component with multiple defects that are distributed throughout its surface such as a water-etch defect, pictured in Fig. 2 (right). Water-etch is the consequence of water entering the bearing through an orifice or broken seal and degrading the grease. This grease degradation leads to increased metal-to-metal friction, which in turn causes the rolling surfaces of the bearing components to wear away at

✉ Constantine Tarawneh
constantine.tarawneh@utrgv.edu

¹ University Transportation Center for Railway Safety (UTCRS), University of Texas Rio Grande Valley (UTRGV), Edinburg, TX, USA

² Hum Industrial Technology, Inc, St. Louis, MO, USA

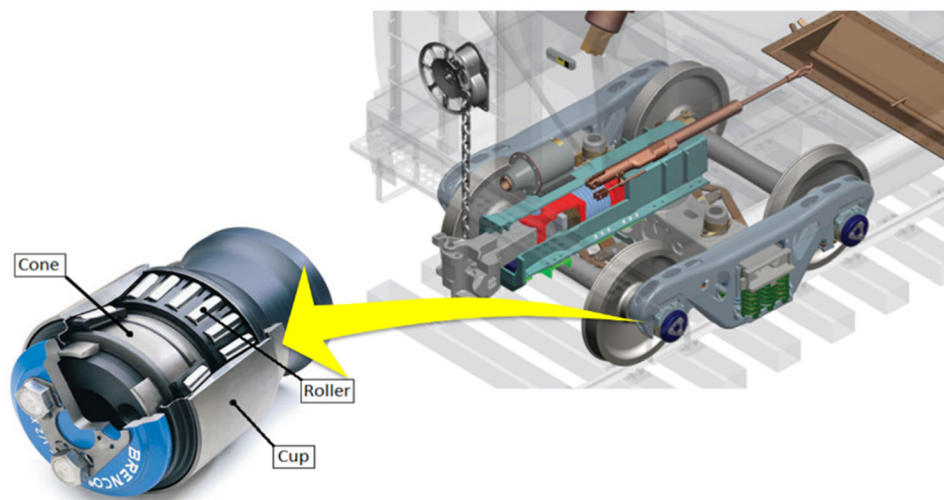


Fig. 1 Fundamental components of a typical tapered-roller bearing used in freight railcars [1]



Fig. 2 Example of a localized defect (left) and distributed defect (right)

a faster rate due to the decreased effectiveness of the lubricant.

Pits, cracks, and spalls are usually the result of subsurface inclusions or defects close to the surface of the raceway (i.e., within 500 μm below the raceway surface). Types of subsurface inclusions include small voids and contaminants and are the result of the supplier's manufacturing processes. Subsurface inclusions close to the surface of the raceway turn into localized defects through rolling contact fatigue (RCF). Under constant RCF, microcracks appear around the subsurface inclusions and propagate to the raceway surface, causing metal to flake off and creating spalls on the raceway. These metal flakes get enmeshed in the grease and begin creating new dents and pits on the raceway surfaces.

Bearings have a nominal service life of a minimum three million rail kilometers (two million rail miles) and are expected to fail due to fatigue. Precautions such as bearing condition monitoring systems are put in place to prevent catastrophic bearing failure.

The study presented in this paper focuses on the implementation of accelerometers mounted on a specially machined bearing adapter to compare the bearing's vibration signatures against two speed-dependent thresholds developed from over a decade of laboratory and field testing. Additionally, spectral analysis is performed to determine the defective component within the bearing assembly. The accuracy and efficacy of this system has been verified through extensive laboratory testing conducted under varying speeds and loads and bearing conditions. This system was also tested at the Transportation Technology Center, Inc. (TTCI) in Pueblo, Colorado to verify the accuracy and reliability of the system in rail service. Note that there are other uses of this system, such as wheel impact load detection, but are outside the scope of this paper.

2 Technology review

2.1 Wayside bearing condition monitoring systems

The railroad industry currently utilizes two types of wayside detection systems to monitor the health of freight railcar bearings in service: The trackside acoustic detection system (TADSTM) and the wayside hot-box detector (HBD). While the two systems use different methods to determine if a bearing is defective, the principle is the same. These wayside bearing condition monitoring systems collect and analyze data from the bearings as they pass by the sensors. If the bearing is operating above a predetermined threshold, the conductor is notified to stop and the wheel-axle assembly with the defective bearing is replaced. This requires the train to be stopped for several hours which is very costly and can potentially cause temperature-sensitive freight to spoil.

2.1.1 Trackside acoustic detection system (TADSTM)

TADSTM, pictured in Fig. 3, uses wayside microphones to detect high-risk defects in bearings and alert the conductor as the train passes by the system. A “growler” is an example of a high-risk defect in which spalls occupy about 90% of the bearing component’s rolling surface. The system is proficient in determining end-of-life bearings but fails to identify bearings with defects at their early stages of development. Moreover, there are less than 20 systems in service throughout the USA and Canada, and TADSTM is not proficient in detecting inner ring (cone) defects [3, 4]. The latter facts suggest that many bearings may spend their entire service life without passing through a TADSTM station, and many other bearings with relatively small defects will go undetected as they pass through TADSTM.

2.1.2 Hot-box detectors (HBDs)

HBDs, shown in Fig. 4, are the most utilized bearing condition monitoring systems in operation in North



Fig. 3 Photograph of a TADSTM site [2]

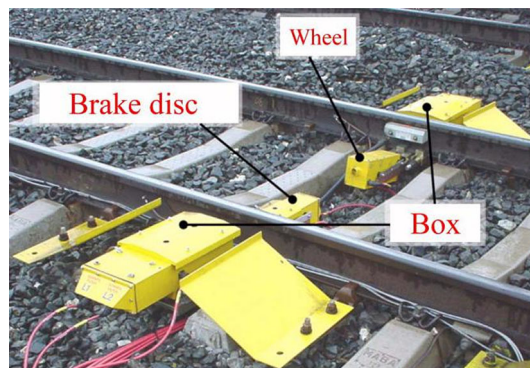


Fig. 4 Example of an HBD site [5]

America with over 6000 in use [3]. They are usually placed 40-rail km (25 mi) apart, with some positioned 64-rail km (40 mi) apart on rail lines with less traffic. HBDs use non-contact infrared sensors to measure the temperature radiated from the bearings, wheels, axles, and brakes as they roll over the detector. The HBD will alert the train operator of any bearings running at temperatures greater than 94.4 °C (170 °F) above ambient conditions or any bearings operating at a temperature greater than 52.8 °C (95 °F) above the temperature of the bearing that shares the same axle [6].

Some railroads have adapted the use of HBDs to look for bearings that are operating at temperatures above the average temperature of all bearings on the same side of the train, as detected by multiple HBDs. These bearings are classified as “warm trended” bearings and are flagged without triggering an HBD alarm [6]. They are subsequently removed from service for later disassembly and inspection. In some cases, bearings with relatively large defects can run at normal operating temperatures for tens of thousands of kilometers before any abnormality in their operating temperature can be observed [7]. In certain instances, a bearing’s raceway may deteriorate rapidly and cause excessive roller misalignment. The misaligned rollers generate frictional heating, which can weaken an axle in 60–135-s and may lead to a catastrophic derailment depending on the traveling speed of the train and the load it is carrying [8].

Several laboratory and field studies have concluded that the accuracy and reliability of the HBD temperature readings are inconsistent [9–11]. The measured temperatures can be significantly different from the actual operating temperature of the bearing. The latter can be attributed to several factors such as the class of the railroad bearing and its position on the axle relative to the position of the wayside detector, and environmental conditions that can affect the IR sensor measurements among other possible factors. Inconsistent HBD readings caused 124 severely defective bearings not to be detected by these condition

monitoring systems in the USA and Canada from 2010 to 2018, 117 of which resulted in costly catastrophic derailments totaling approximately \$36 million in damages [12]. Attempts by some railroads to remedy the situation by using statistical analysis, run on HBD-acquired data, to set out bearings that run hotter than the average temperature of bearings along one side of the train have resulted in a significant increase in the number of non-verified bearings removed from service. In fact, about 40% of the bearings removed from service in the period from 2001 to 2007 were found to have no discernible defects according to data collected by Amsted Rail. The removal of non-verified bearings has resulted in many costly train stoppages and delays.

2.2 Onboard bearing condition monitoring systems

As evident by the accident statistics summarized earlier, axle journal burn-off can occur between HBD locations, which highlights the need for an advanced onboard bearing condition monitoring system that can detect the onset of defect initiation, track its deterioration, and alert train operators and railroads of impending bearing failures well in advance so that proactive maintenance can be scheduled.

Over the past three decades, a few onboard bearing health monitoring systems have been introduced to the market. A description of these systems along with their advantages and disadvantages is presented hereafter.

2.2.1 SMART-BOLT™

The SMART-BOLT™ system was developed in the 1990s to detect and alert the locomotive engineer of an impending overheated bearing. The system replaces one of the three bearing end cap bolts with a thermal sensor-bolt and consists of a passive thermo-mechanical sensor/actuator, transmitter, and a power source [13]. The SMART-BOLT™ has an alarm-point threshold of 121 °C (250 °F) to prevent catastrophic damage to the bearing seal. Once above this threshold, the bolt extends a piston and deploys an antenna to transmit a radio signal of an overheated bearing to the locomotive engineer. The extended antenna allows inspectors to quickly identify which bearing is potentially defective.

However, this product has two drawbacks: it does not track bearing condition over time; therefore, it cannot aid in setting proactive maintenance schedules, and it requires an authorized party to manually reset the thermal actuator, even in instances of false positives.

2.2.2 Onboard wireless sensor node (WSN)

An alternative to the SMART-BOLT™ is the onboard wireless sensor node (WSN). The WSNs can continuously collect and transmit temperature data to a central monitoring unit (CMU) computer onboard the railcar. The CMU can then wirelessly transmit the analyses via satellite or cellular network to the locomotive engineer. This allows the engineer to take any preventative measures to avoid possible derailments [14]. The main drawback of this system is that it only records and transmits the bearing temperature. As discussed earlier, temperature is not a good indicator of bearing health as it cannot identify the presence of defects at an early stage because bearing temperature usually increases dramatically when the defect has grown to a relatively large size, and thus, failure is imminent. In other words, this system does not afford the rail operator enough time to schedule proactive maintenance because once a bearing has triggered any of the alarm thresholds, the train must be stopped immediately so that the entire wheel-axle assembly (which includes the two bearings) can be replaced.

2.2.3 Timken Guardian™ bearing

The Timken Guardian™ bearing is the latest onboard condition monitoring product on the market. The Guardian™ bearing can measure operational speed, temperature, and vibration of the bearing assembly. These sensors can detect bearing and wheel failure, along with stuck hand brakes. This system is self-powered and contains an internal microprocessor that analyzes the data and transmits the results via wire or wirelessly [15]. However, when a possible defect is detected, the wheel-axle assembly must be removed so a thorough inspection can be conducted. This process does not afford the railcar owner the option to reuse any of the suspension components or the Guardian™ Bearing. This forces the railcar owner to invest more capital into a new high-priced Guardian™ bearing.

2.2.4 Proposed onboard bearing condition monitoring system solution

An ideal onboard bearing condition monitoring system is one that is cost-effective, easily replaceable, and can accurately detect and monitor bearing defect growth at an early stage, among other performance metrics. Currently, researchers at the University Transportation Center for Railway Safety (UTCRS) have developed a battery-powered sensor module that can measure the operating load, temperature, and vibration levels within a bearing and wirelessly transmit the data to a central computing unit that analyses the acquired data and sends the analysis results to

the cloud. The transmitted results would inform railcar owners of any possible defects and provide an estimate of the residual life of a defective bearing measured in remaining mileage of operation. Unlike other onboard systems, the estimated residual life would allow the railcar to remain in service for longer periods avoiding unnecessary and costly train stoppages and delays since the defects would be detected at their early stages of development.

3 Experimental setup and procedures

The UTCRS dynamic bearing testers, housed at UTRGV, were used to perform all relevant laboratory testing for this study for the purpose of replicating bearing operation in freight railcars. Table 1 lists the four classes of railroad bearings that the two testers can accommodate. Each tester is equipped with a hydraulic cylinder that allows each bearing to be loaded up to 150% of their maximum operational load as stated in the Association for American Railroads (AAR) standards. Note that full load for a class F or K bearing corresponds to 153 kN (34.4 kips) per bearing. The data provided in this paper was collected utilizing three loading conditions, namely 17% of full load, which simulates an empty railcar, 100% of full load, which corresponds to a fully loaded railcar, and 110% of full load, which simulates an overloaded railcar.

The test rigs are equipped with a 22 kW (30 hp) variable speed motor which allows the bearings to be tested at the different simulated train velocities listed in Table 2. The motors are controlled by variable frequency drives (VFD) that accurately maintain the desired angular speeds to within 0.5%. Motor power and angular speed data are collected from the VFD every 20 s and are used to check for any abnormal operation during testing. The bearings are air-cooled utilizing two industrial-size fans that produce an air stream traveling at an average speed of 6 m/s (13.4 mph).

Table 1 Bearing classes with dimensions and AAR rated load capacities at full load (100%)

Bearing class	Size (mm)	Load (kN)
Class E	152 × 279	117
Class F	165 × 305	153
Class G	178 × 305	169
Class K	165 × 229	153

Table 2 Typical speeds used to perform the experiments for this study

Axle speed (rpm)	Track speed (mph)	Track speed (km/h)
280	30	48
327	35	56
373	40	64
420	45	72
467	50	80
498	53	85
514	55	89
560	60	97
618	66	106
699	75	121
799	85	137

3.1 Laboratory test rigs

3.1.1 Four-bearing test rig (4BT)

The 4BT, pictured in Fig. 5, can accommodate four class F, K, G, or E railroad bearings pressed onto a customized test axle.

To replicate field service conditions, only data collected from the middle two bearings (B2 and B3) were used for this study since they are both top loaded. Thus, the middle two bearing adapters were machined to accept two customized 70 g ADI ADXL001-70BEZ accelerometers (placed in the outboard smart adapter (SA) and mote (M) locations), one 500 g PCB 355B02 accelerometer (placed in the outboard radial (R) location), two K-type bayonet thermocouples, and one regular K-type thermocouple aligned with the two bayonet thermocouples and placed midway along the bearing cup width, held tightly by a hose clamp. Figure 6 shows the SA, M and R location of the accelerometers on the modified bearing adapter (left) as well as the thermocouple locations (right).

Note that the sensors pictured in Fig. 6 are part of the initial wired version of the onboard condition monitoring system that was used to develop and optimize the wireless version pictured in Fig. 7. The wireless onboard condition monitoring system has been extensively validated and proven to produce identical results to those obtained by the wired version shown in Fig. 6.

3.1.2 Single bearing test rig (SBT)

The SBT, depicted in Fig. 8, accommodates a single railroad tapered-roller bearing (classes E, F, G, or K) in a cantilever setup, which closely mimics the bearing loading conditions on freight railcars. An AdapterPlusTM bearing adapter was specially machined to accept four 70 g ADI

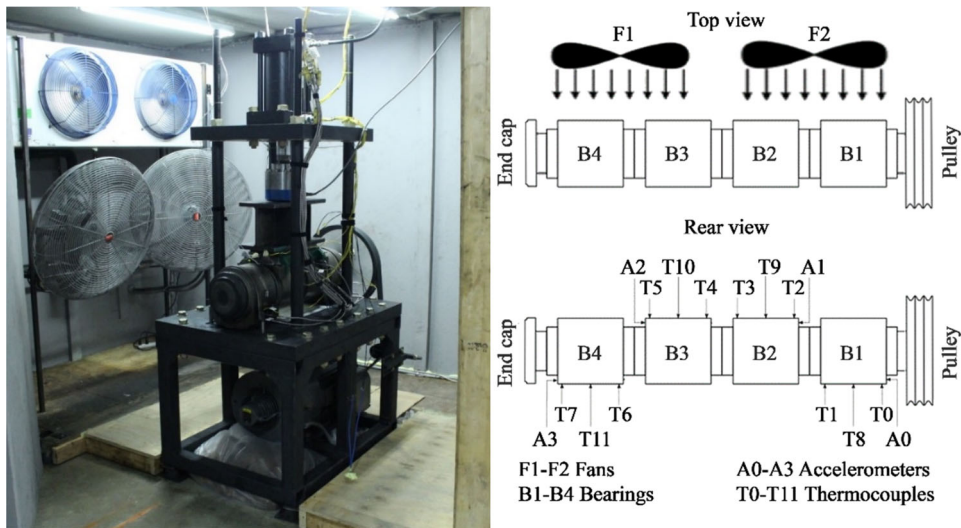


Fig. 5 Four-bearing test rig (4BT) and schematic representation of instrumentation

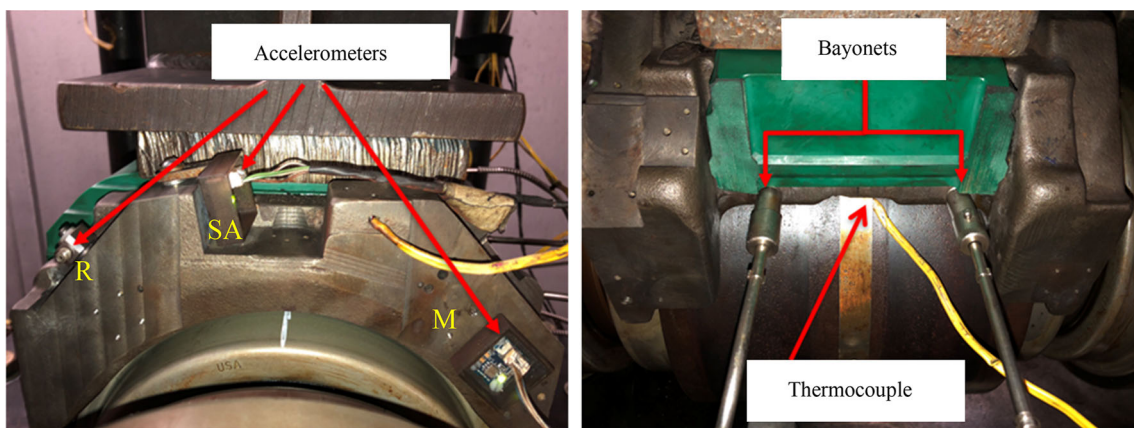


Fig. 6 Wired version of the onboard condition monitoring system showing accelerometer locations on the machined bearing adapter (left) as well as thermocouple locations (right)

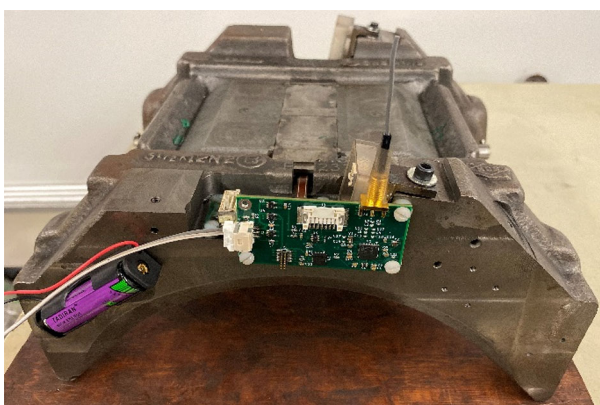


Fig. 7 A picture of the wireless onboard condition monitoring system powered by a battery pack and affixed to the bearing adapter

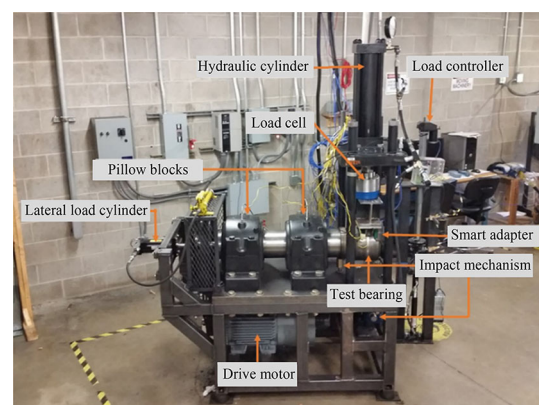


Fig. 8 Single bearing test rig (SBT)

ADXL accelerometers (placed in SA and M locations at the inboard and outboard sides of the bearing), one 500 g PCB accelerometer (placed in the R location on the outboard side), and four K-type bayonet thermocouples (two inboard and two outboard). In addition to the four thermocouples affixed to the bearing adapter, there are seven K-type thermocouples placed equidistantly around the circumference of the bearing cup and held in place tightly via a hose clamp, as shown in Fig. 9.

3.2 Load controllers

All test rigs used for this study utilize hydraulic cylinders to apply load to the bearings. External load controllers were fabricated and used to counteract the effects of thermal expansion and contraction of the hydraulic fluid in the load cylinders. These external load controllers consist of a 38 mm (1½-inch) bore hydraulic cylinder driven by a linear actuator. The linear actuator is powered by a DC motor that transforms rotational energy into translational energy using a threaded rod and a gearbox. The DC motor is controlled by one of two circuits: a LabVIEW™-based circuit or an Arduino-based circuit. Both circuits allow the applied bearing load to be within ± 1560 N (350 lbs) of the desired load. Each circuit has a manual override to initially set the desired applied bearing load.

3.2.1 LabVIEW™-based load controller circuit

Data taken from a 445 kN (100 kip) Interface® load cell is transferred to a computer running LabVIEW™ every twenty-seconds via a National Instruments (NI) USB-6008 data acquisition (DAQ) system. An error loop in the program regulates the load the hydraulic cylinder applies based on the values provided by the load cell every 2 min. If the load error exceeds the aforementioned tolerance of ± 1560 N (350 lbs), an NI USB-6211 sends a five-volt

pulse signal via the digital output port to the load motor controller until the force is within the specified tolerance. This system allows for different load ramps to be applied automatically.

3.2.2 Arduino-based load controller circuit

The Arduino-based system utilizes a five-volt hydraulic pressure transducer affixed to the hydraulic cylinder on the test rigs and an Arduino UNO to process the data. If the pressure in the hydraulic cylinder correlates to a load outside of the load tolerance, the Arduino sends a five-volt signal to the load motor to adjust the applied load until it is within the specified tolerance.

3.3 Data acquisition system (DAQ)

A NI cDAQ-9174 programmed using LabVIEW™ was utilized to record and collect all the data for this study. A NI 9213 card was used to collect the K-type thermocouple temperature data at a sampling rate of 128 Hz for half a second, in twenty-second intervals. A combination of an NI 9239, an NI USB-6008, and an NI 9234 cards was used to record and collect the accelerometer data for this study at a sampling rate of 5120 Hz for 16-s, in 10-min intervals. The root-mean-square (RMS) of the accelerometer data was then used to perform the analysis presented in this paper.

3.4 Field test

In 2015, the UTCRS research team, in collaboration with Amsted Rail Engineers, conducted a proof of concept field test at the Transportation Technology Center, Inc. (TTCI) in Pueblo, Colorado. The primary objective of the field test was to validate the accuracy and reliability of the onboard accelerometer-based condition monitoring system in detecting defective bearings. A locomotive towing a business car and an instrumented freight railcar (empty 1 day and fully loaded the second day) along different TTCI tracks at speeds ranging from 48 to 105 km/h (30–65 mph) provided the field test data for this study. The data acquisition system was set up in the business car. Figure 10 is a picture of the business car, and the freight railcar as the UTCRS research team was completing the instrumentation in preparation for the field test at TTCI.

It is important to note that this field test was implemented as a blind test, i.e., the UTCRS researcher in charge of analyzing the data did not know the type and location of the four defective bearings within the freight railcar. Out of the eight railroad bearings on the instrumented freight railcar, four were defect-free (healthy), two contained outer ring (cup) spalls, and two had inner ring (cone) spalls.

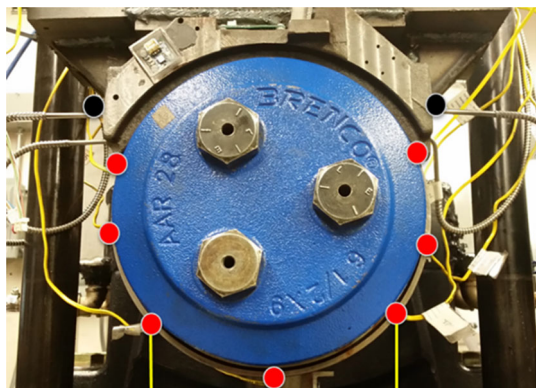


Fig. 9 Placement of thermocouples on the railroad bearing (red dots represent the locations of the regular K-type thermocouples and black dots represent the locations of the bayonet K-type thermocouples)



Fig. 10 A picture of the business car and the freight railcar being instrumented for the field test at the Transportation Technology Center, Inc. (TTCI)

Figure 11 provides the locations of the healthy and defective bearings on the instrumented freight railcar. Table 3 displays the conditions of the bearings along with their defect sizes. All defects were placed on the inboard raceway, whereas all the sensors were placed on the outboard side of the bearing adapter. This provides a worst-case scenario where the defect is the furthest away from the sensors.

The field test utilized two different TTCI tracks to evaluate the difference in results when the train travels over a smooth versus a rough track. One 70 g and one 500 g accelerometer were mounted on each bearing adapter at the SA and R locations (refer to Fig. 6), respectively. In the field test, temperature data were collected at a sampling rate of 128 Hz for half a second, in fifteen second intervals, whereas the accelerometer data were collected continuously at a rate of 5556 Hz. All instrumentation was powered by the locomotive.

Table 3 Bearing conditions and their mounted locations on the test freight railcar at TTCI

Position	Bearing condition	Defect size (cm ²)
L1	Cone defect inboard (IB)	14.2
R1	Control (healthy)	–
L2	Control (healthy)	–
R2	Cup defect inboard (IB)	34.2
L3	Cup defect inboard (IB)	8.4
R3	Control (healthy)	–
L4	Control (healthy)	–
R4	Cone defect inboard (IB)	3.9

4 Bearing defect detection algorithm

Based on the laboratory testing, a field implementation version of the bearing defect detection algorithm was developed to identify the presence of raceway defects at the early stages of their initiation while also determining the defect location and estimating its size. The temperature sensor of the wireless condition monitoring module and a GPS chip installed in the central computing unit record the bearing operating temperature and the train traveling speed, respectively. Currently, the algorithm is set to trigger when the train is operating at speeds of at least 64 km/h (40 mph) or the bearing operating temperature is above 93 °C (200 °F). Note that these thresholds can be adjusted as needed through programming. Once the algorithm is triggered, the accelerometer embedded within the onboard sensor module collects 4-s of vibration data at a sampling rate of 5 kHz (20,000 data points). The onboard sensor modules are affixed to the bearing adapter, and there are eight modules mounted per freight railcar (one for each bearing). The root-mean-square (RMS) of the vibration data is calculated and a single g-value is output. Figure 12

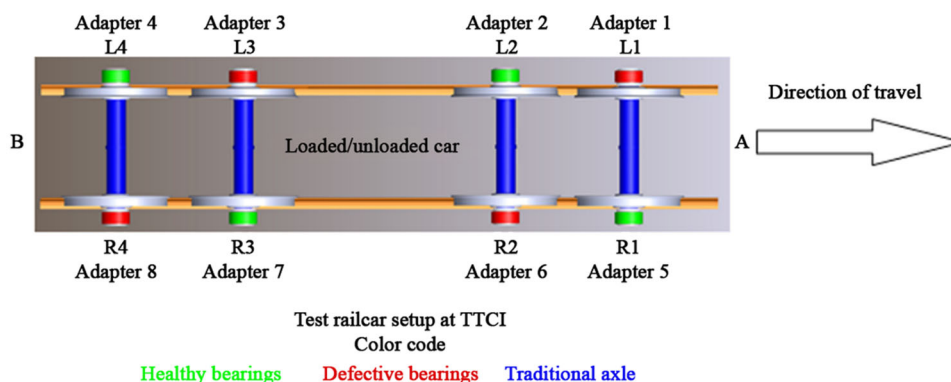


Fig. 11 Schematic diagram describing the test freight railcar setup at TTCI

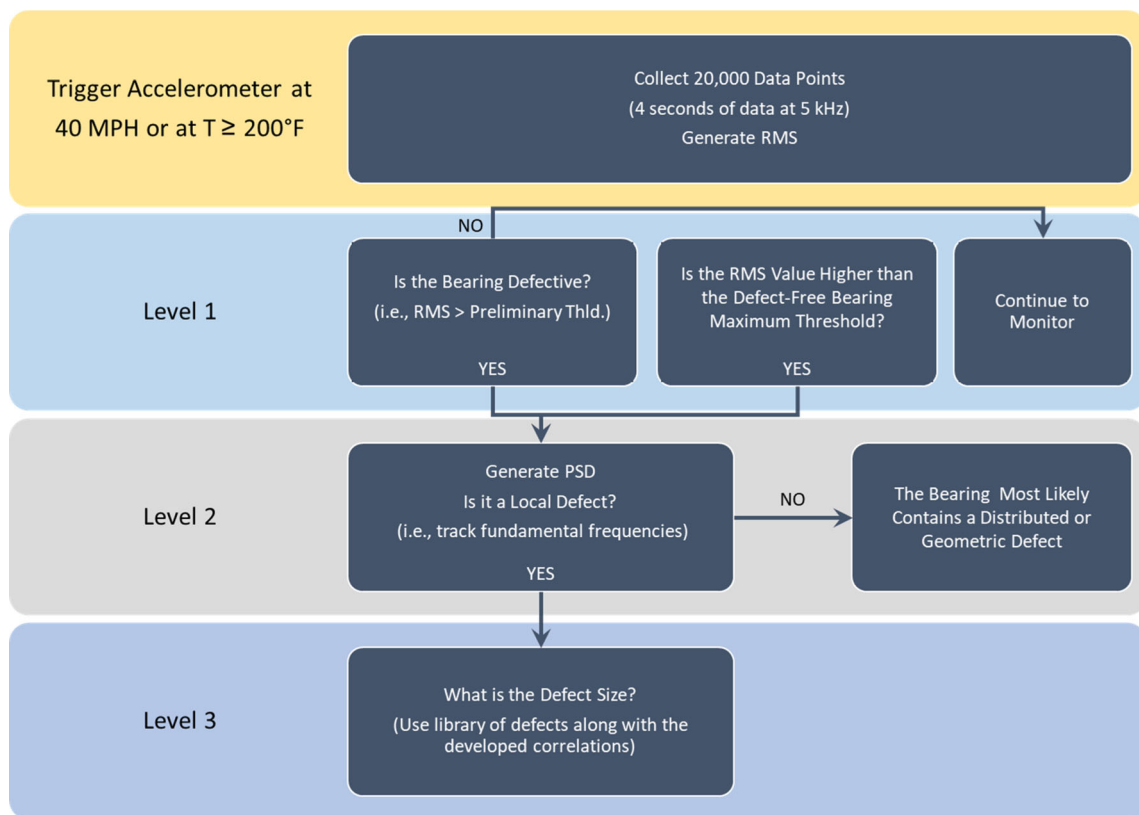


Fig. 12 Flowchart of the proposed algorithm [16]

provides a brief description of each level within the algorithm.

4.1 Level 1: Is the bearing defective?

Level 1 of the algorithm determines the condition of the bearing. Two speed-dependent thresholds were developed using a library of defect-free bearing vibration signatures acquired through laboratory testing. The RMS values acquired prior to Level 1 analysis are compared against these thresholds.

4.1.1 Preliminary threshold

Preliminary threshold (T_p) was selected based on a statistical analysis of several possible thresholds based on correlations of speed (V) and the mean RMS values of defect-free (healthy) bearing vibration signatures. Table 4 summarizes all eleven possible thresholds and their corresponding percentages. These possible thresholds were based on the following: μ , $\mu \pm \frac{1}{2} \sigma$, $\mu \pm \sigma$, and upper and lower bounds of the 90%, 95%, and 99% confidence intervals (CI) for the mean RMS, where the confidence intervals represent a proportion of the samples averaged

which contain the true mean. The variables μ and σ represent, respectively, the mean and standard deviation of defect-free bearing RMS values for each speed. The ideal T_p should minimize the amount of defective bearings below the threshold while also limiting the amount of defect-free bearings above the threshold.

Based on the results listed in Table 4 [16], the upper bound of the 95% confidence interval threshold was selected as the T_p due to summation of both percentages being the lowest across all possible thresholds. Equation (1) gives T_p as a function of V :

$$\begin{cases} T_p = 7.331 \times 10^{-2}V - 9.059 \times 10^{-2} & V \text{ in km/h} \\ T_p = 4.556 \times 10^{-2}V - 9.059 \times 10^{-2} & V \text{ in mph} \\ T_p = 4.879 \times 10^{-3}V - 9.059 \times 10^{-2} & V \text{ in rpm} \end{cases} \quad (1)$$

If the calculated RMS value is below the T_p , then the bearing is categorized defect-free, and the data collection continues as discussed earlier. Conversely, if the calculated RMS value of a bearing is greater than the T_p , then the bearing is determined to be possibly defective, and the algorithm will proceed to Level 2.

Table 4 Percentages of defect-free and defective bearing RMS values that fall above and below possible threshold correlations, respectively

Possible threshold	Defect-free bearing RMS values above possible threshold (%)	Defective bearing RMS values below possible threshold (%)
Upper bound 99% CI (μ)	13.8	33.2
Upper bound 95% CI (μ)	19.3	27.4
Upper bound 90% CI (μ)	21.8	26.6
$\mu + \sigma$	26.8	23.5
$\mu + \frac{1}{2} \sigma$	33.9	20.5
μ	43.8	15.8
$\mu - \frac{1}{2} \sigma$	52.1	11.6
$\mu - \sigma$	61.0	8.5
Lower bound 90% CI (μ)	65.3	6.9
Lower bound 95% CI (μ)	72.6	6.2
Lower bound 99% CI (μ)	87.9	3.5

4.1.2 Maximum threshold

Maximum threshold (T_{\max}) was developed so that all bearings with an RMS value above it are flagged as defective. The T_{\max} is based on a correlation between the maximum defect-free bearing RMS values for each speed data set versus the speed (V). The upper bound of the 45% CI, plotted in Fig. 13, provided the most conservative threshold for which no defect-free bearings would be mis-categorized as defective. Equation (2) gives T_{\max} as a function of train/axle speed V :

$$\begin{cases} T_{\max} = 1.788 \times 10^{-1} V - 1.008 & V \text{ in km/h} \\ T_{\max} = 1.111 \times 10^{-1} V - 1.008 & V \text{ in mph} \\ T_{\max} = 1.119 \times 10^{-2} V - 1.008 & V \text{ in rpm} \end{cases} \quad (2)$$

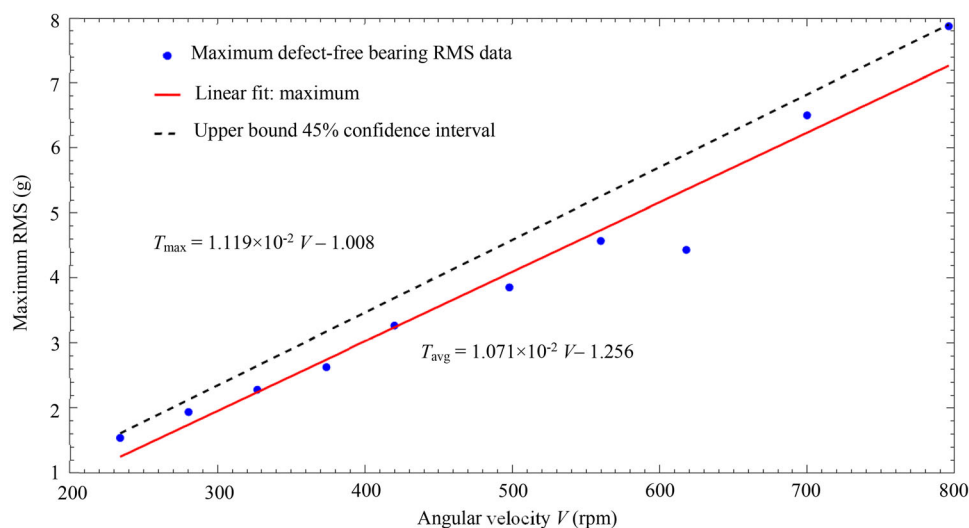
Note that the idea behind using both a preliminary threshold and a maximum threshold is to be able to

categorize bearings into: (1) bearings that are potentially defective, and (2) bearings that are definitely defective.

4.2 Level 2: What is the defect type?

Level 2 analysis of the algorithm determines the defect type (local or distributed/geometric) present within the identified defective bearing. The algorithm utilizes frequency-domain analysis and creates power spectral density (PSD) plots, where a PSD, given in Eq. (3), is the square of the absolute magnitudes in the frequency domain, $X(f)$, after which six rotational frequencies are tracked using Eqs. (4)–(9) [17]:

$$\text{PSD} = |X(f)|^2, \quad (3)$$

**Fig. 13** Plot of maximum defect-free bearing RMS values versus angular velocity

$$\omega_{ir} = \omega_o, \quad (4)$$

$$\omega_{cg} = \left(\frac{R_{ir}}{R_{ir} + R_{or}} \right) \omega_{ir}, \quad (5)$$

$$\omega_r = \left(\frac{R_{ir}}{D_r} \right) \omega_{ir}, \quad (6)$$

$$\omega_{out} = 23\omega_{cg}, \quad (7)$$

$$\omega_{in} = 23 \times (\omega_{ir} - \omega_{cg}), \quad (8)$$

$$\omega_{rd} = \left(\frac{R_{or}}{R_r} \right) \omega_{cg}. \quad (9)$$

Equations (4)–(9) are based on the axle rotational speed (ω_o) and the radii and diameters of several tapered-roller bearing components. R_{ir} and R_{or} refer to the radii of the inner ring (cone) and outer ring (cup), respectively, whereas R_r and D_r refer to the radius and diameter of the roller, respectively. The parameters ω_{ir} , ω_{cg} , and ω_r refer to, respectively, the rotational velocities of the inner ring (which is equal to ω_o since the inner ring is press-fit onto the axle), the cone assembly cage, and the roller. Equations (7)–(9) are the defect frequencies of the tapered-roller bearing and correspond to a defect on the outer ring (ω_{out}), inner ring (ω_{in}), and roller (ω_{rd}), respectively. The number 23 in Eqs. (7) and (8) refers to the 23 rollers within each cone assembly. Determining these three defect frequencies is essential to properly categorize the type of defect within the bearing. A defective component will exhibit a spike in power at its corresponding defect frequency in a PSD plot, whereas a healthy bearing will show no major spikes. Figure 14 gives examples of each type of bearing condition and its corresponding defect frequency and harmonics up to 1000 Hz.

These defect frequencies and harmonics are then used to calculate the normalized defect energy (NDE) for each bearing in order to categorize the defect [17]. The NDE is computed by taking the square of the sum of areas under a specific defect frequency (cup, cone, or roller) and its harmonics within the PSD divided by the total amount of harmonics within a specified frequency range. However, laboratory and field testing have shown that the calculated frequencies were slightly shifted from the actual frequencies, causing improper NDE calculations. These shifts can be caused by the slight differences in tolerances of the components as well as any speed variations or component slipping. A hunting range (h_r) was incorporated to mitigate these shifts in the fundamental frequencies. The hunting range is a function of the resolution (rs) of the spectrum and varies with the rotational speed of the axle (ω_o). The resolution is calculated by dividing the sampling frequency

by the number of data points used to generate the frequency plot.

Low speed	$\omega_o < 355 \text{ rpm}, h_r = \pm rs \times 6.$
Medium speed	$355 \text{ rpm} \leq \omega_o < 610 \text{ rpm}, h_r = \pm rs \times 10.$
High speed	$610 \text{ rpm} \leq \omega_o, h_r = \pm rs \times 15.$

Once the actual fundamental frequencies are found, the normalized defect energy is then calculated. Equations (10)–(12) are used to calculate the normalized defect energy for each defect type. The parameter n in Eqs. (10)–(12) is the total number of harmonics for a specific defect frequency within the desired frequency range. An integration range ($i_r = rs \times 3$) was set to capture most or all of the harmonics of the fundamental defect frequencies up to 1000 Hz. Figures 15 and 16 depict, respectively, a visual representation of the hunting range used to determine the actual fundamental frequency and the integration range used to calculate the normalized defect energy:

$$\text{NDE}_{\text{cup}} = \left(\frac{\sum_{i=1}^n \int_{i\omega_{out}-i_r}^{i\omega_{out}+i_r} |X(f)|^2 df}{n} \right)^2, \quad (10)$$

$$\text{NDE}_{\text{cone}} = \left(\frac{\sum_{i=1}^n \int_{i\omega_{in}-i_r}^{i\omega_{in}+i_r} |X(f)|^2 df}{n} \right)^2, \quad (11)$$

$$\text{NDE}_{\text{roller}} = \left(\frac{\sum_{i=1}^n \int_{i\omega_{rd}-i_r}^{i\omega_{rd}+i_r} |X(f)|^2 df}{n} \right)^2. \quad (12)$$

In order to determine the defect type (localized, distributed, or geometric) within the identified defective bearing, the highest normalized defect energy of the three defect types must be divided by the sum of all three normalized defect energies, as shown in Eq. (13). If the ratio falls below 50% on an identified defective bearing, then the bearing either has a distributed defect on multiple components of the bearing, or it contains a geometric defect, or is a falsely flagged healthy bearing (not common). If the ratio of the highest normalized defect energy to the sum of all three normalized defect energies is above 50%, then the bearing has a localized defect on the component with the highest normalized defect energy and the algorithm proceeds to Level 3 analysis, where the size of the defect is estimated using developed defect-size correlations [18]. However, for brevity, only Level 1 and Level 2 analyses are provided in this paper. A demonstration on the use of Level 3 analysis can be found elsewhere [19].

$$\frac{\max(\text{NDE}_{\text{cup,cone,roller}})}{\text{NDE}_{\text{cup}} + \text{NDE}_{\text{cone}} + \text{NDE}_{\text{roller}}} \times 100\% \geq 50\%. \quad (13)$$

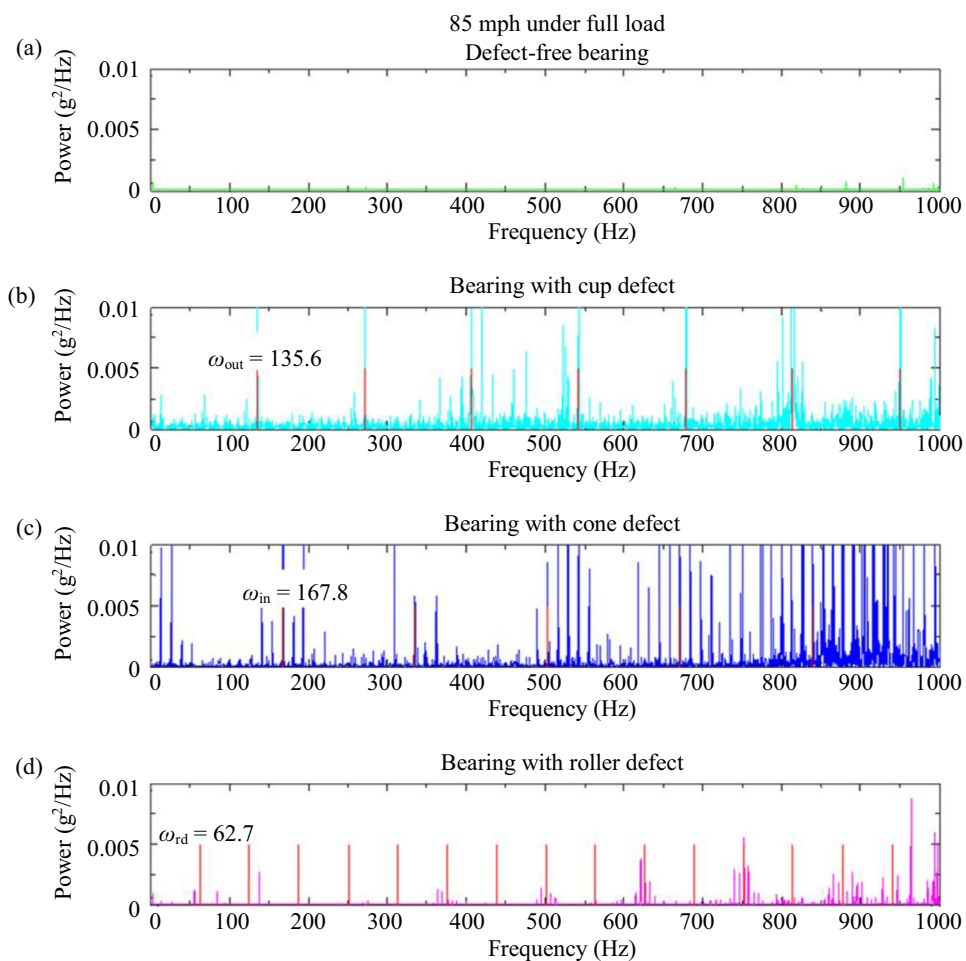


Fig. 14 Frequency spectrum plots (0–1000 Hz) of **a** defect-free (healthy) bearing, **b** outer ring (cup) defect, **c** inner ring (cone) defect, and **d** roller defect. The vertical red lines in this figure represent the defect frequencies and their harmonics up to 1000 Hz

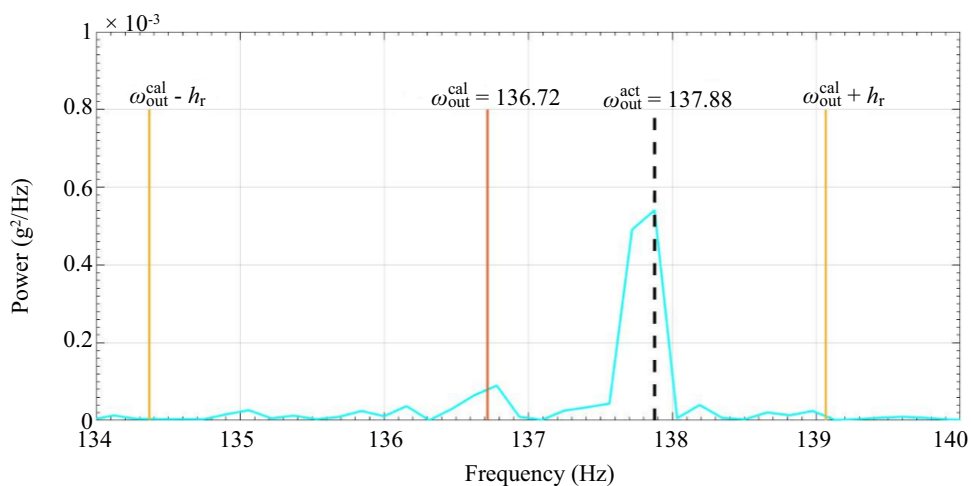


Fig. 15 Example of using the hunting ranges to determine the actual fundamental defect frequency

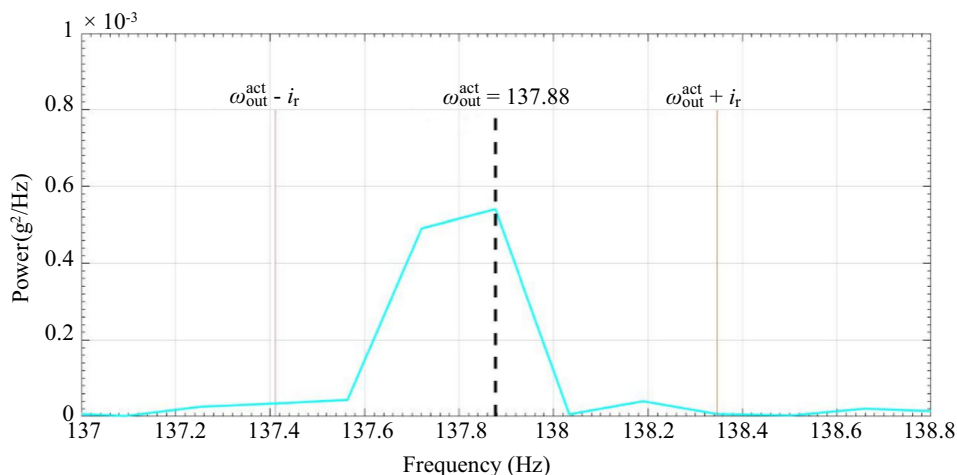


Fig. 16 Example of using the integration ranges to calculate the normalized defect energy for each fundamental defect frequency

5 Results and discussion

To demonstrate the efficacy of the proposed onboard condition monitoring system, validation testing examples that were obtained from both laboratory and field testing at TTCI are given hereafter. In the first example, a bearing with a defective outer ring (cup) that was tested in the laboratory is presented, whereas, in the second example, a bearing with a defective inner ring (cone) that was field tested at the TTCI rail tracks is examined. These examples were carefully chosen to showcase the effectiveness and accuracy of the proposed system in identifying relatively small defects that are in their early stages of development both in a laboratory setting and in field service.

To obtain one representative value for each speed and load combination during laboratory testing, the mean of the RMS and NDE values for the final 2 h of data acquired (i.e., twelve data points) were calculated for Level 1 and Level 2 analyses, respectively. In field testing, the latter was accomplished by obtaining the mean of all the RMS and NDE values after speed reached steady state. All Level 1, Level 2, and temperature results will be summarized in tables. RMS values above the T_p in the Level 1 tables will be italicized, whereas the RMS values above the T_{max} in Level 1 tables and percentages of the NDE values above 50% in Level 2 tables will be bolded.

5.1 Laboratory experiment 200: cup defect

In laboratory Experiment 200, a class K bearing with a pitted inboard cup (outer ring) raceway was run in the B2 position on the 4BT (refer to Fig. 5). The initial defect, pictured in Fig. 17 (left), propagated throughout the experiment to a final size of 8.98 cm² (1.39 in²), as shown in Fig. 17 (right).

The final defect size of 8.98 cm² corresponds to approximately 2.4% of the 367.28 cm² (56.93 in²) total area of one cup raceway in a class K bearing. To accelerate the testing and simulate a worst-case scenario, the region of the pit on the cup was placed directly under the full load path and the bearing was run at 137 km/h (85 mph) and 110% of full load representing an overloaded railcar.

5.1.1 Level 1 analysis: Is the bearing defective?

Figure 18 depicts the vibration and temperature profiles for bearing 2 (B2) and bearing 3 (B3) throughout Experiment 200. The control bearing correlation in Fig. 18 refers to a previous study for which the average operating temperatures above ambient (ΔT) for healthy (defect-free) bearings at several speeds for empty and fully loaded railcars were acquired [7]. Note that bearings tend to operate at temperatures above the control bearing threshold regardless of bearing health at the beginning of experiments as the freshly packed grease breaks in. The ambient temperature was held at 20 °C (68 °F). Tables 5 and 6 provide the average values of the final 2 h of each loading condition during the experiment.

Initially, the vibration levels within B2 were slightly below the T_{max} . After the 150-h mark, B2 vibration levels started to increase reaching levels that are noticeably above the T_{max} , signifying a defective bearing. This fluctuation in vibration levels is indicative of defect growth. As the defect grows, metal debris from the cup raceway is circulated throughout the bearing during operation. This causes an increase in roller misalignment and is represented by an increase in vibration. However, as the debris gets crushed by the rotating rollers, the vibration levels start to decline. This cycle repeats itself every time the defect deteriorates. Since the vibration levels within B2 exceeded the T_{max} at

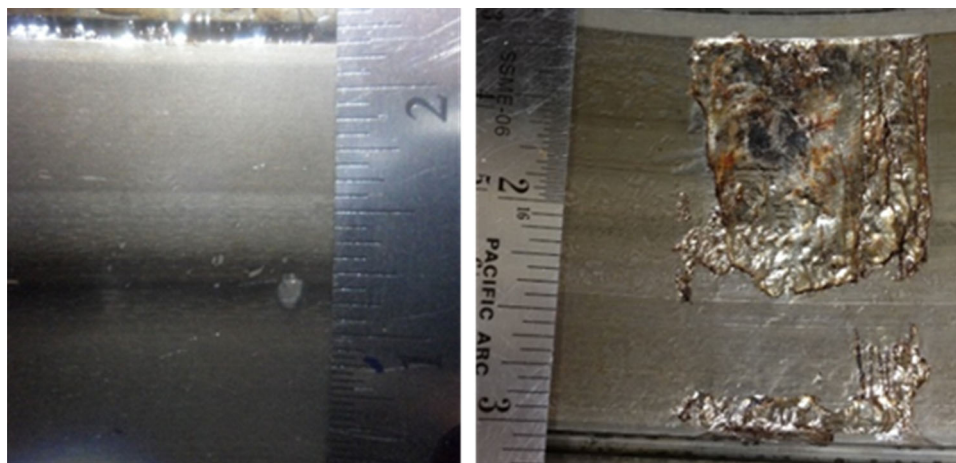


Fig. 17 Initial pitting on cup raceway (left) and resulting cup spall (right) (ruler is in inches)

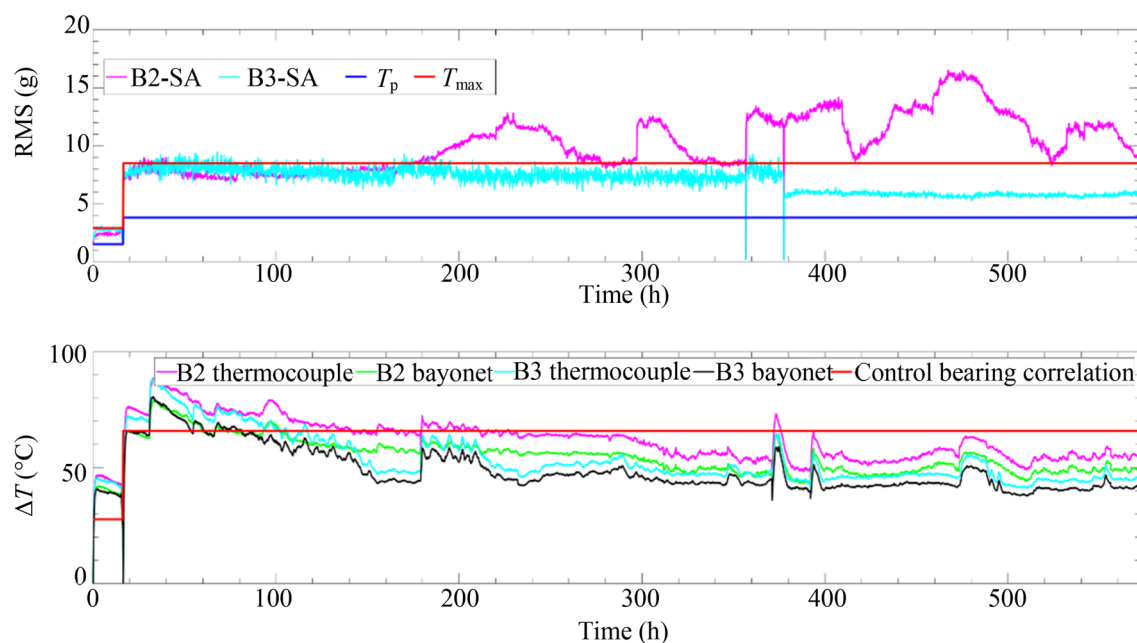


Fig. 18 Vibration and temperature profiles for bearing 2 (B2) and bearing 3 (B3) during Experiment 200

Table 5 Average values of bearing 2 (cup defect) during Experiment 200

Track speed (km/h)/(mph)	Load (%)	ΔT (°C)	Control ΔT (°C)	RMS (g)	Preliminary threshold, T_p (g)	Maximum threshold, T_{max} (g)
56/35	100	41	29	2.5	1.5	2.9
137/85	110	48	66	9.8	3.8	8.5

Table 6 Average values of bearing 3 (healthy) during Experiment 200

Track speed (km/h)/(mph)	Load (%)	ΔT (°C)	Control ΔT (°C)	RMS (g)	Preliminary threshold, T_p (g)	Maximum threshold, T_{max} (g)
56/35	100	40	29	2.2	1.5	2.9
137/85	110	41	66	5.8	3.8	8.5

137 km/h (85 mph), B2 proceeds to Level 2 analysis. The vibration levels within B3 remained above the T_p but below the T_{max} . Upon teardown and visual inspection, B3 did not have any visible defects and was determined to be healthy.

5.1.2 Level 2 analysis: What is the defect type?

Since B2 was classified as defective in Level 1 analysis, the NDE (“max/sum”) value is calculated. The results in Table 7 show the Level 2 analysis for B2 using the proposed method in Eq. (13). The analysis performed at a simulated train speed of 137 km/h (85 mph) and 110% of full load resulted in a NDE_{cup} of 99.6%, which confirms that the bearing has a defect on its cup (outer ring) raceways. Consequently, the analysis proceeds to Level 3 in which the defect size is estimated using the developed defect size correlations [18].

5.2 Field test validation

To demonstrate the efficacy of the proposed onboard condition monitoring system in rail service, it was implemented in a field test performed at the TTCI rail tracks as described in Sect. 3.4 of this paper. This field test was successful, and the individuals performing the analysis of the acquired data were able to accurately identify all four defective bearings as well as the location of the defect (i.e., whether it is on the cone or cup of the bearing). The analysis performed on the bearing located in the L1 position (refer to Fig. 11 and Table 3) is presented here. This bearing had a defective cone (inner ring) with a total spalled area of 14.2 cm² (2.2 in²), as pictured in Fig. 19. This bearing was chosen because current wayside detection systems are not proficient in identifying cone defects. Hence, being able to reliably detect cone spalls in rail service is advantageous. Photographs of the defective cone in the L1 Bearing are shown in Fig. 19. Test speeds varied between 64 km/h (40 mph) and 105 km/h (65 mph), and test loads alternated between 17% (empty railcar) and 100% (fully loaded freight railcar).

5.2.1 Level 1 analysis: Is the bearing defective?

Table 8 provides a summary of the percentages of steady-state data that were found to have RMS values above the T_{max} for each speed and load iteration. The results show that the L1 Bearing was accurately classified as defective in

almost all the steady-state data acquired during the TTCI field test for every load and speed combination. The lack of data acquired at full load and speeds above 89 km/h (55 mph) is because the testing facility at TTCI limited the speed of fully loaded railcars to no more than 89 km/h (55 mph). Since the bearing was correctly identified as defective, the analysis proceeds to Level 2 to identify the defective component within the bearing assembly.

5.2.2 Level 2 analysis: What is the defect type?

Level 2 analysis was performed on the defective L1 Bearing. A summary of the results under unloaded and fully loaded conditions are provided in Table 9. From the results, it is evident that the algorithm has correctly identified the defective component within the bearing for all speed and load iterations. The data also suggest that the normalized defect energy (NDE) for the defective component increases with load and speed. This means that the algorithm is proficient in identifying defective bearings and the type of defect within the bearing at higher speeds and full load.

6 Conclusions and future work

Wayside condition monitoring systems currently in use in North America are reactive in nature, and numerous derailments have resulted from overheated bearings that went undetected. To combat this, an onboard bearing condition monitoring system was developed that can accurately and reliably detect bearings with surface defects smaller than 4% of the total raceway surface area by analyzing the vibration signatures emitted by the bearings.

The devised onboard condition monitoring system has undergone rigorous laboratory testing and targeted field testing at the Transportation Technology Center, Inc. (TTCI) at Pueblo, Co. A wireless version of the system has also been developed and tested extensively yielding results identical to those of the wired version. The authors are working with a private rail industry partner to deploy this wireless system in a couple of Class I and II railroads and gather data to further validate the efficacy and accuracy of the system in detecting defective bearings in regular rail service. Moreover, the acquired vibration data from these planned field tests will be correlated to wheel impact load detector (WILD) data to determine whether the onboard

Table 7 Level 2 analysis of Bearing 2 for Experiment 200 using NDE

Track speed (km/h)/(mph)	Load (%)	NDE $\frac{\max}{\text{sum}} \times 100\%$	Defective component
137/85	110	99.6	Cup

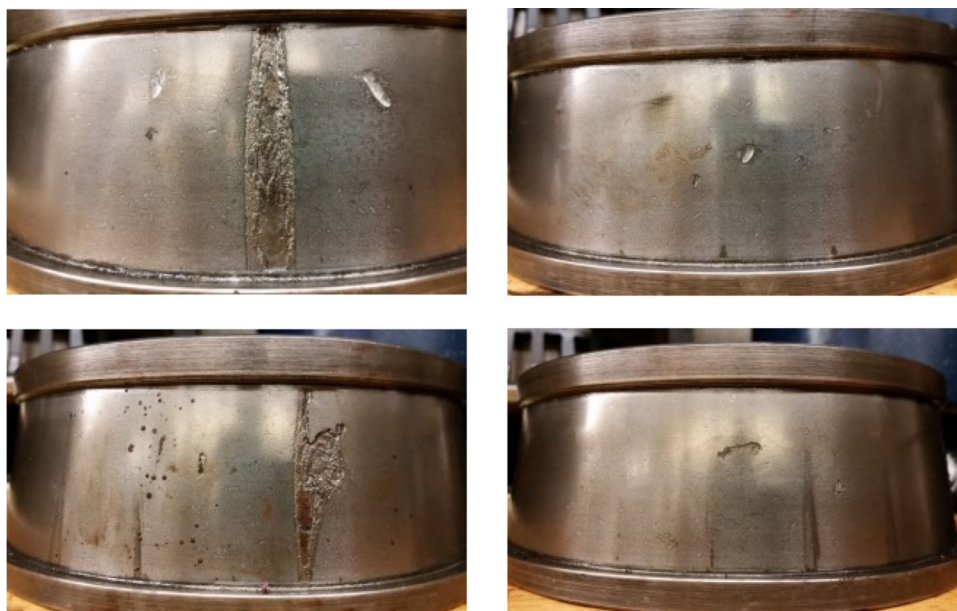


Fig. 19 Photographs of L1 bearing cone defect (refer to Fig. 11 and Table 3)

Table 8 Percentages of steady-state data with RMS values greater than the T_{\max} for 17% load (empty railcar) and 100% load (full railcar)

Speed (km/h)/(mph)	Empty railcar (17% load) (%)	Fully loaded railcar (100% load) (%)
64/40	97	100
80/50	100	100
89/55	100	100
97/60	100	–
105/65	100	–

Table 9 Average normalized defect energy (NDE) values during steady-state operation for each load and speed combination and the corresponding defective component

Speed (km/h)/(mph)	Average NDE $\frac{\max}{\text{sum}} \times 100\%$		Defective component
	Empty railcar (17% load)	Fully loaded railcar (100% load)	
64/40	51	62	Cone
80/50	78	68	Cone
89/55	70	72	Cone
97/60	83	–	Cone
105/65	87	–	Cone

condition monitoring system can also be utilized to detect high wheel impact loads.

Finally, the proposed system is proactive in nature and can detect the onset of bearing failure at early stages. Based on the vibration levels within the bearing, the system will provide an estimate for the remaining mileage of operation, giving the rail operators and car owners enough time to schedule regular maintenance and avoid unnecessary and costly train stoppages and delays. The authors hope that

this onboard condition monitoring system will enhance the way the rail industry performs rolling stock health monitoring and will result in reduced catastrophic derailments and associated human and capital loss.

Acknowledgements The authors wish to acknowledge the financial support from the University Transportation Center for Railway Safety (UTCRS) which was funded through USDOT Grant No. DTRT13-G-UTC59. The authors also want to thank Amsted Rail engineers who provided many of the test bearings for this study.

Funding This study was made possible by funding provided by The University Transportation Center for Railway Safety (UTCRS), through a USDOT Grant No. DTRT 13-G-UTC59.

Disclosure statement Any opinions, findings, conclusions, or recommendations are those of the authors and do not necessarily reflect the views of the USDOT or Amsted Rail Industries.

Open Access This article is licensed under a Creative Commons Attribution 4.0 International License, which permits use, sharing, adaptation, distribution and reproduction in any medium or format, as long as you give appropriate credit to the original author(s) and the source, provide a link to the Creative Commons licence, and indicate if changes were made. The images or other third party material in this article are included in the article's Creative Commons licence, unless indicated otherwise in a credit line to the material. If material is not included in the article's Creative Commons licence and your intended use is not permitted by statutory regulation or exceeds the permitted use, you will need to obtain permission directly from the copyright holder. To view a copy of this licence, visit <http://creativecommons.org/licenses/by/4.0/>.

References

- Freight Car Components Amsted Rail. <https://www.amstedrail.com/products-services/freight-car-components>
- Marketing, Nuthouse. Advanced Rail Engineering. Etion Digitise. <http://www.ansysrail.co.za/trackside-solutions/>
- Stewart MF et al (2019) An implementation guide for wayside detector systems. Federal railroad administration. <http://railroads.dot.gov/elibrary/implementation-guide-wayside-detector-systems>
- Anderson GB (2007) Acoustic detection of distressed freight car roller bearing. In: Proceedings of the JRCICE spring technical conference, Pueblo, Colorado, USA
- Schöbel A, Pisek M, Karner J (2006) Hot box detection systems as a part of automated train observation in Austria. In: Towards the competitive rail systems in Europe, pp 157–161
- Karunakaran S, Snyder TW (2007) Bearing temperature performance in freight cars. In: Proceedings bearing research symposium, sponsored by the AAR research program in conjunction with the ASME RTD Fall conference, Chicago, Illinois, USA
- Tarawneh C, Sotelo L, Villarreal A, et al (2016) Temperature profiles of railroad tapered roller bearings with defective inner and outer rings. In: Proceedings of the ASME joint rail conference, Columbia, South Carolina, USA
- Wang H, Conry TF, Cusano C (1996) Effects of cone/axle rubbing due to roller bearing seizure on the thermomechanical behavior of a railroad axle. *J Tribol* 118:311–319
- Mealer A, Tarawneh C, Crown S (2017) Radiative heat transfer analysis of railroad bearings for wayside hot-box detector optimization. In: Proceedings of the ASME joint rail conference, Philadelphia, Pennsylvania, USA
- Aranda J (2018) Radiative heat transfer analysis of railroad bearings for wayside thermal detector optimization. Master's Thesis, University of Texas Rio Grande Valley
- Tarawneh C, Aranda J, Hernandez V et al (2020) An investigation into wayside hot-box detector efficacy and optimization. *Int J Rail Transp* 8(3):264–284
- 3.10-Accident Causes\Federal Railroad Administration, Office of Safety Analysis. <https://safetydata.fra.dot.gov/OfficeofSafety/publicsite/Query/inccaus.aspx>
- Tabbachi JG, Newman RR, Leedham RC, et al (1990) Hot bearing detection with the SMART-BOLT. In: Proceedings of the ASME/IEEE joint railroad conference, pp 105–110
- Technology. Amsted Digital Solutions, Amsted Rail, Inc., www.amsteddigital.com/technology/. Accessed 26 April 2019
- Rail News - Timken Supplies 'Intelligent' Rail Bearing Technology for FRA Field Test. For Railroad Career Professionals. *Progressive Railroading*, 2004, https://www.progressiverailroading.com/supplier_spotlight/news/Timken-supplies-intelligent-rail-bearing-technology-for-FRA-field-test-6598
- Gonzalez A (2015) Development, optimization, and implementation of a vibration-based defect detection algorithm for railroad bearings. Master's Thesis, University of Texas Rio Grande Valley
- Alvarado IL (2012) Defect detection in railroad tapered-roller bearings using vibration analysis techniques. Master's Thesis, University of Texas-Pan American
- Lima JD (2020) Residual service life prognostic models for tapered-roller bearings. Master's Thesis, University of Texas Rio Grande Valley
- Lima JD, Tarawneh C, Aguilera J, and Cuanang J (2020) Estimating the inner ring defect size and residual service life of freight railcar bearings using vibration signatures. In: Proceedings of the ASME joint rail conference, St. Louis, Missouri, USA